Energy Proceedings
Vol 31, 2023
ISSN 2004-2965

# Mechanistic assessments of NO activation on $WO_3$-promoted $CeO_2$ catalysts and its consequences for low-temperature $NH_3$-SCR

Wenshuo Hu[1 #], Yu Zhang[1 #], Xiaoxiang Wang[2], Weihong Wu[1], Hao Song[1], Shaojun Liu[1*], Xiang Gao[1*]

1 State Key Laboratory of Clean Energy Utilization, Zhejiang University, 38 Zheda Road, Hangzhou, 310027, China

2 Institute of Industrial Ecology and Environment, Zhejiang University, 38 Zheda Road, Hangzhou, 310027, China

*# W.H. and Y.Z. contributed equally to this work*

## ABSTRACT

Ceria has absorbed extensive interests in mediating low-temperature (LT) selective catalytic reduction (SCR) of NOx due to its abundance of surface oxygen species and consequential salient redox property. The mechanistic interpretations of how such redox property contributes to its LT-SCR activity, however, still remain debated. Here, we use a model $WO_3$-promoted $CeO_2$ catalyst ($WO_3/CeO_2$), known as preeminent in LT-SCR reactions, and combine kinetic, characteristic and in situ spectroscopic experiments with theoretical treatments to reveal the mechanistic connections between NO oxidative activation and LT-SCR turnovers. We show that NO oxidation to $NO_2$ is both kinetically (reaction rates: 8~40-fold lower than LT-SCR at 423~523 K) and thermodynamically (reaction free energy at 473 K: ~20 kJ $mol^{-1}$ higher than NO to nitrites) less favorable than NO activation to nitrite intermediates, thus suggesting a relevance of the latter route, rather than NO oxidation to $NO_2$ and subsequent occurrence of fast SCR, to $WO_3/CeO_2$-catalyzed LT-SCR reaction cascade.

**Keywords:** NOx, selective catalytic reduction, ceria, low-temperature, reaction mechanism, NO activation

## 1. INTRODUCTION

As integral to clean energy development, the disposal of exhaust emission has always been emphasized on. NOx abatement has become one of the major objectives of the environmental and health protection framework as a result of both increasing emissions and more stringent regulations. Selective catalytic reduction (SCR) with $NH_3$ is currently a state-of-the-art technology for controlling NOx from mobile and stationary sources. [1-5] In spite of the successful application of $V_2O_5$-$WO_3/TiO_2$ catalysts in coal-fired power plants, their lack of DeNOx efficiency at lower temperatures (e.g., 473 K) has motivated substantial endeavors to enhance LT-SCR activities through developing new catalysts[6-9]. Among these, $CeO_2$ is one of the most eye-catching materials due to its preeminent oxygen storage capacity and ease in forming/repairing surface oxygen-vacancies (Ov), which render superior redox property to $CeO_2$-based catalysts[9-13]. Discussions on how such redox property contributes to their improved LT-SCR activities are still diverging; various proposals, such as promoted NO oxidation to activated NOx intermediates with higher N-states (e.g., nitrites, nitrates)[9, 13-15] or to $NO_2$ so that higher contributions from fast SCR[10, 16-18], have been frequently reported to account for the observed LT-SCR activity enhancement.

Here, we use a model catalyst with $WO_3$ supported on the surface of $CeO_2$, i.e., $WO_3/CeO_2$, a material widely documented as an excellent LT-SCR catalyst [10, 12, 14, 19], and focus on how this catalyst enhances NO oxidative activation, with an attempt to uncover its mechanistic consequence for LT-SCR turnovers. In doing so, we apply an integrated experimental and theoretical approach combining steady-state kinetic, structural characteristic, in situ spectroscopic and chemical trapping measurements with theoretical treatments [density functional theory calculations with corrections of dispersion and Coulomb onsite correlation (DFT+ $U$ + D)]. Such a coordinated strategy enables a detailed comparison of different NO activation routes and reveals that NO activation to nitrite-intermediates is both kinetically and thermodynamically more favorable than NO oxidation to $NO_2$, which may progress the mechanistic insights into LT-SCR redox chemistry over $CeO_2$-based catalysts.

## 2. MATERIALS AND METHODS

### 2.1 Experimental

The $WO_3/CeO_2$ catalysts and the NOx trapper, i.e., $BaO/Al_2O_3$, used in this work were prepared by the impregnation method, with ammonium metatungstate [$(NH_4)_6H_2W_{12}O_{40}\cdot xH_2O$, Aladdin] and $Ba(CH_3COO)_2$ (Sigma-Aldrich) solution impregnating the $CeO_2$ support (Sigma Aldrich, $S_{BET}$=30 $m^2$ $g^{-1}$) and γ-$Al_2O_3$ powders (Aladdin), respectively. The theoretical $WO_3$ loading is 3% wt., corresponding to a surface density of ~2.56 W $nm^{-2}$, and the theoretical Ba-loading is 16% wt. [13]. Additional details can be found in ref. [13].

Steady-state kinetic measurements were conducted in a fixed-bed quartz reactor (ID=7 mm). For standard SCR tests, equimolar NO and $NH_3$ (350 ppm), 4% $H_2O$ and 5% $O_2$ were used at a total flow rate of ~111.1 $cm^3$ $g_{cat}^{-1}$ $s^{-1}$ (STP), and effluent gas species were measured by an infrared analyzer (MKS MultiGas 2030). For NO oxidation tests, 500 ppm NO, 5% $H_2O$ and 5% $O_2$ were used at a lower flow rate of ~55.6 $cm^3$ $g_{cat}^{-1}$ $s^{-1}$ (STP) to ensure detectable NO conversions. For measurements of kinetic orders of NO, $NH_3$ and $O_2$ in LT-SCR reactions (473 K), varying concentrations of each species while keeping the others constant based on a reference state of NO=$NH_3$=500 ppm, $O_2$=$H_2O$=5%, a flow rate of ~111.1 $cm^3$ $g_{cat}^{-1}$ $s^{-1}$ (STP) were performed. Before each test, an oxidative treatment of 5% $O_2$ + 5% $H_2O$ was performed at 773 K for 5 h to stabilize the catalysts loaded.

X-ray photoelectron spectra (XPS) were recorded on a Thermo Scientific ESCALAB 250Xi with Al Kα source of 1486.6 eV, calibrated by the C 1s binding energy (BE) of 284.8 eV [4, 7]. The in situ infrared (IR) spectra were collected on a Nicolet 6700 spectrometer. Details on IR measurements can be found in ref. [13].

### 2.2 Computational

A $p(2\times2)$ surface unit cell was built by cutting bulk $CeO_2$ in (1 1 1) orientation, as detailed in [13], on which a monomeric $WO_4H_2$ cluster was deposited to simulate the experimental $WO_3/CeO_2$ catalyst. Periodic density functional theory (DFT) calculations were executed with the Vienna Ab initio Simulation Package (VASP)[20]. The Generalized Gradient Approximation (GGA) exchange–correlation functional by Perdew, Burke, and Ernzerhof (PBE) with a plane-wave cutoff of 600 eV, an effective Hubbard-type $U$ parameter of 5 eV for Ce 4$f$ electrons and the DFT-D3 scheme with Becke–Johnson damping accounting for long-range van der Waals interactions (i.e., PBE+$U$+D) were used to treat the $WO_4H_2/CeO_2$ (1 1 1) system [21-26]. Total electronic energy and atomic forces were converged to $10^{-6}$ eV and 0.02 eV $Å^{-1}$, respectively, with 2×2×1 $k$ points sampling of the first Brillouin zone[13, 27]. DFT-computed energetics were further translated to Gibbs free energies at 473 K and standard pressure (0.1 MPa) on replacing low-frequency modes by 2/3 of translational and rotational entropies and enthalpies of relevant gas-phase molecules[13, 28].

## 3. RESULTS AND DISCUSSION

### 3.1 Steady-state kinetic measurements

Fig.1 shows standard SCR kinetics over $WO_3/CeO_2$, reported in terms of normalized 1st-order rates of NO (see kinetic discussions in Fig.3) and conversions of NO and $NH_3$ (the inset). Equivalent NO and $NH_3$ conversions are observed at all tested temperatures, consistent with the standard SCR stoichiometry and thus confirming the absence of side reactions in the present case. Mixing $WO_3/CeO_2$ with $BaO/Al_2O_3$, an effective NOx storage material able to store unstable nitrites and/or nitrite-precursors[13, 29-31] in the form of $Ba(NO_2)_2$, shows no significant effect on measured SCR kinetics, therefore rationalizing the use of $BaO/Al_2O_3$ in following mechanistic investigations.

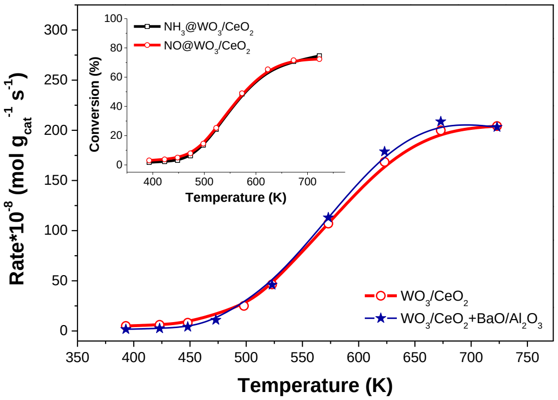

Fig.1. Standard SCR kinetics (1st-order NO rates, per mass) on $WO_3/CeO_2$ and mechanical mixture of $WO_3/CeO_2$+$BaO/Al_2O_3$. Inset: conversions of NO and $NH_3$ on $WO_3/CeO_2$.

We also tested NO oxidation kinetics on $WO_3/CeO_2$, as shown in Fig.2. In general, rates of NO oxidation and $NO_2$ formation (far from equilibrium: the approach to equilibrium $\eta < 10^{-5}$) are very low: 8~40-fold lower than the standard SCR rates in the range of 423~523 K. Such a significant discrepancy between NO oxidation and standard SCR suggests a kinetic irrelevance of these two reactions, which questions the argument of attributing rate enhancements observed in LT-SCR to promoted NO oxidation and consequential higher contributions from fast SCR[10, 16-18] on the present $WO_3/CeO_2$ catalyst.

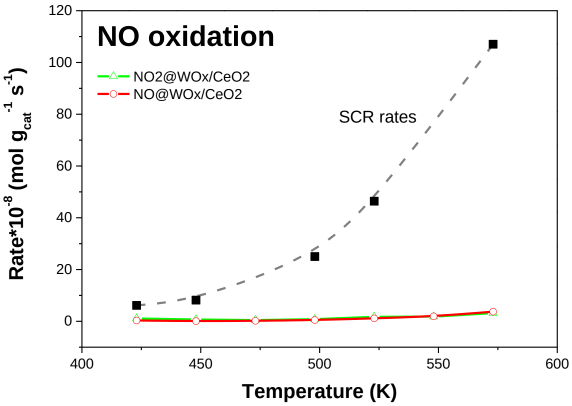

Fig.2. NO oxidation rates on $WO_3/CeO_2$. For comparison, rates of standard SCR were also included.

Steady-state standard SCR rates can be described using the following rate expression:

$$r_{SCR} = k \cdot P_{NO}^{\alpha} \cdot P_{NH_3}^{\beta} \cdot P_{O_2}^{\gamma} \qquad \text{(Eq.1)}$$

in which kinetic orders α, β and γ were determined experimentally, as illustrated in Fig.3. The measured 0th-order dependence on $NH_3$ ($\beta \approx 0$, black in Fig.3a) and 1st-order dependence on NO ($\alpha \approx 1$, red in Fig.3a) at 473 K are consistent with literature reports[32] for vanadia-based catalysts, which suggests a surface bound state for $NH_3$ while a gaseous or weakly bound state for NO during LT-SCR over the present $WO_3/CeO_2$. Further, the kinetic order of $O_2$ is small ($\gamma \approx 0.2$, Fig.3b), indicating that adsorbed oxygen species are abundant on the surface of $WO_3/CeO_2$ at such percentage levels of gas-phase $O_2$. This observation is in line with the known preeminent oxygen storage capacity of ceria materials, and further reflects that redox reactions, such as NO activation, are predominately occurring on the catalyst surface.

In the following, we use characterization techniques to directly examine the surface structure of $WO_3/CeO_2$.

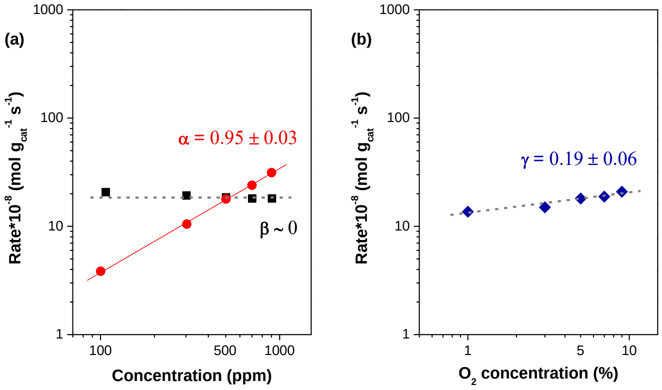

Fig.3. Steady-state kinetic measurements of reaction orders for (a) NO (red) and $NH_3$ (black), (b) $O_2$ at 473 K. Reference condition: $NO=NH_3=500$ ppm, $O_2=H_2O=5\%$. The errors of α and γ represent 95% confidence intervals.

### 3.2 *Structural characterizations*

XPS analysis was performed to probe the surface atomic structure of $WO_3/CeO_2$ and unpromoted $CeO_2$ (impregnated by deionized $H_2O$ using identical synthesis procedure). Fig.4a shows the spectra of O 1s and their deconvolution results, referred to as the surface-active oxygen at 532–531 eV ($O_\alpha$) and the lattice oxygen at 530–529 eV ($O_\beta$) [12, 14], with the former species being more active in oxidation reactions. The relative $O_\alpha$ ratio, calculated as $O_\alpha/(O_\alpha+O_\beta)$, is similar on the two samples (36% vs. 38%) and is indeed much higher than that for commercial $V_2O_5$-$WO_3/TiO_2$ catalysts (~20%) [4, 7], thus consistent with the characteristic feature of abundant surface oxygen species on $CeO_2$ and further suggesting its dominating role in forming $O_\alpha$. Such an abundance of $O_\alpha$ is also consistent with the kinetic order of $O_2$ ($\gamma \approx 0.2$) discussed in Fig.3. Similarly, the Ce 3d spectra are nearly identical on $WO_3/CeO_2$ and unpromoted $CeO_2$ (Fig.4b). The deconvoluted spectra labelled as u''', u'', u, v''', v'' and v are due to the $3d^{10}4f^0$ state of $Ce^{4+}$, while v' (marked in red) is for the $Ce^{3+}$ $3d^{10}4f^1$ [10-12]; their relative $Ce^{3+}$ ratios, i.e., $Ce^{3+}/(Ce^{3+}+Ce^{4+})$, are essentially the same (12% vs. 11%). These results indicate that the low $WO_3$ deposition used in this work does not affect distinctly the surface atomic structure of $CeO_2$.

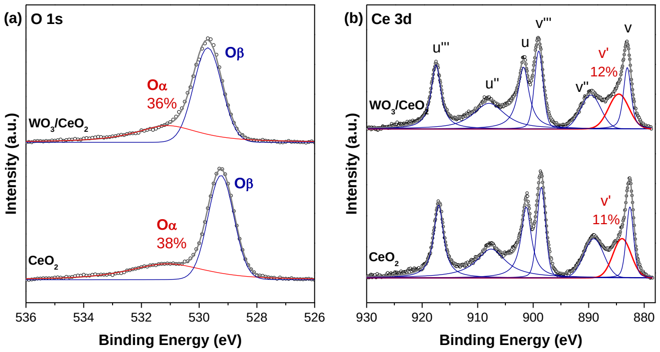

Fig.4. XPS spectra of (a) O 1s and (b) Ce 3d of $WO_3/CeO_2$ and unpromoted $CeO_2$.

### 3.3 *In situ IR and chemical trapping studies*

Fig.5a illustrates in situ IR spectra of NO adsorption at 473 K on $WO_3/CeO_2$: in this test, $O_2$ was not included to refrain gas-phase NO oxidation to $NO_2$ and to focus on contributions from catalyst active sites, as discussed above. A single peak at ~1610 $cm^{-1}$, due to activated NOx adspecies such as adsorbed $NO_2$[9] or nitrites[13], appears upon NO feeding. Such activated NOx products have N oxidation states higher than +2, thus their appearance suggesting the oxidative activation of NO on $WO_3/CeO_2$. Besides, a negative band at ~2001 $cm^{-1}$, assigned to the 1st overtone of surface W=O[5, 33], is also visible in Fig.5a, indicating a consumption/coverage of W=O sites during NO adsorption. We also integrated these two bands (1610 and 2001 $cm^{-1}$) and obtained a synchronized temporal evolution (inset in Fig.5a). This observation, together with the absence of bands at < 1600 $cm^{-1}$ registered for NO adsorption on unpromoted $CeO_2$,[34] suggests that the activated NOx adspecies and W=O groups are closely correlated and further that NO oxidative activation may occur on the W=O site.

To further investigate the NO activation process, we mixed $WO_3/CeO_2$ with $BaO/Al_2O_3$ and executed identical NO adsorption tests (Fig.5b): in this way, we are able to examine the possible unstable activated products that are generated during NO exposure but not detected by the IR spectra. Apparently, the overall scenario differs significantly from the case of $WO_3/CeO_2$ alone (Fig.5a); now multiple bands are resolved, with a pronounced one at ~1230 $cm^{-1}$ (along with a shoulder at 1311 $cm^{-1}$) being the dominating feature. According to literature IR results, bands at 1230 $cm^{-1}$ are attributed to the $\nu_{asym}$ of ionic nitrites[30, 31], and are also compatible with the DFT calculated frequency of HONO (1225 $cm^{-1}$) [13]. Note that $BaO/Al_2O_3$ alone has been confirmed to be inert in activating NO[13, 29-31] and that $BaO/Al_2O_3$ is segregated from $WO_3/CeO_2$, these observations thus infer an oxidative activation of NO on the $WO_3/CeO_2$ component to an unstable and mobile nitrite-precursor intermediate, which is undetected on $WO_3/CeO_2$ alone but can shuttle between the two phases and then gets stabilized on nearby $BaO/Al_2O_3$, presumably as Ba-nitrites through e.g., $2HONO + BaO \rightarrow Ba(NO_2)_2 + H_2O$.[13, 29-31]

Next, we turn to DFT calculations to further explore the NO oxidative activation at a molecular level.

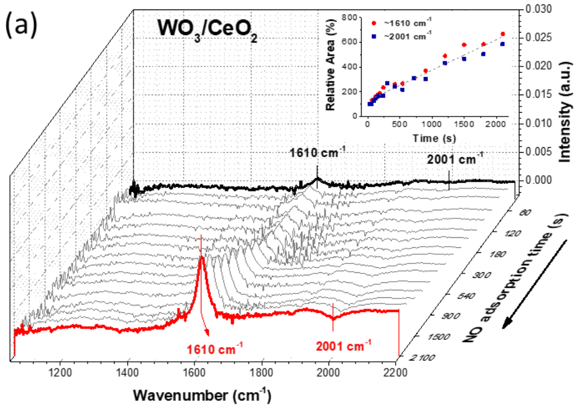

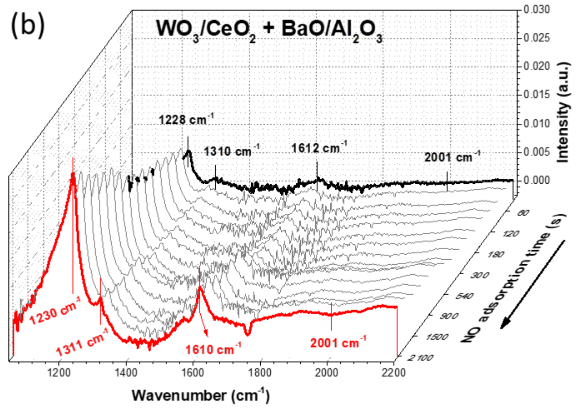

Fig.5. In situ IR spectra of NO adsorption on preoxidized (a) $WO_3/CeO_2$ and (b) mechanical mixture of $WO_3/CeO_2$ + $BaO/Al_2O_3$, mass ratio of $WO_3/CeO_2$ to $BaO/Al_2O_3$ =2:1. Total flow rate=1.67 $cm^3\ s^{-1}$ (STP), T=473 K, NO=350 ppm.

### *3.4 DFT calculations*

As documented in the literature[13, 29-31, 35], NO oxidative activation can form gaseous nitrite precursors like HONO, $N_2O_3$ and/or $NO_2$, with the latter species also being in the form of $N_2O_3$ in a large excess of NO:

$$NO + NO_2 \leftrightarrow N_2O_3 \qquad (R.1)$$

These nitrite precursors are able to facilely react with $BaO/Al_2O_3$ to more stable $Ba(NO_2)_2$:

$$2HONO + BaO \rightarrow Ba(NO_2)_2 + H_2O \qquad (R.2)$$

$$N_2O_3 + BaO \rightarrow Ba(NO_2)_2 \qquad (R.3)$$

which explains the chemical trapping results in Fig.5.

Fig.6 shows the PBE+*U*+D derived free energies for different NO activation routes. An initial reference state before NO activation is represented by a free NO close to the $WO_4H_2$ cluster (left). After NO attacking one of the $W^{6+}$-OH groups, a gaseous HONO species is formed with an endergonic free energy of +20 kJ $mol^{-1}$ (central left). Alternatively, NO can also bind to the terminal W=O group and form a “W-ONO” structure with a more favorable free energy of +7 kJ $mol^{-1}$ (central right). This result aligns with the spectroscopic observation (Fig.5a) of synchronized evolution of W=O and activated NOx species, and further suggests a correspondence of this “W-ONO” structure to the 1610 $cm^{-1}$ bands. Moreover, oxidation state analysis reveals that one of the surface $Ce^{4+}$ has been reduced to $Ce^{3+}$, while the $W^{6+}$ remains unchanged, directly indicating that such NO adsorption on W=O already activates NO to an adsorbed nitrite (N oxidation state: +3), analogous to previous findings on a similar $VOx/CeO_2$ catalyst [13]. Further desorbing this adsorbed nitrite to a gaseous $NO_2$ needs an additional free energy of +22 kJ $mol^{-1}$ (right in Fig.6), suggesting that such a desorption step is energetically unfavorable. Taken together, the free energies here indicate that the route of NO activation to surface adsorbed nitrites (+7 kJ mol$^{-1}$) prevails over those of NO to HONO (+20 kJ mol$^{-1}$) and to gaseous $NO_2$ (+29 kJ mol$^{-1}$). Noteworthy, such unfavorable NO oxidation to $NO_2$ is consistent with the experimentally observed low activity of NO oxidation, even given the test was performed in the presence of percentage levels of gas-phase $O_2$ (Fig.2).

The presence of $BaO/Al_2O_3$, however, can readily consume gas-phase activated NOx products (R.1 − R.3), which favors the overall reaction energies and in turn promotes NO oxidative activation in the chemical trapping experiment (Fig.5b) [13, 29]. Further, from a mechanistic perspective, another SCR reactant—$NH_3$—can also facilely scavenge these NOx products and is expected to be even more effective as it is a gas-phase molecule that has a much closer contact with $WO_3/CeO_2$ surface than mechanically mixed $BaO/Al_2O_3$ powders; these two facts favor the adsorbed nitrite as a plausible intermediate in LT-SCR over $WO_3/CeO_2$, because of its lowest free energy cost (+7 kJ mol$^{-1}$) and well-known reactivity with $NH_3$ to $N_2$:[7, 30, 31, 35]

$$NO_2^- + H^+ + NH_3 \rightarrow N_2 + 2H_2O \qquad \text{(R.4)}$$

Further explorations on the LT-SCR redox chemistry are ongoing and will be discussed in details in forthcoming works.

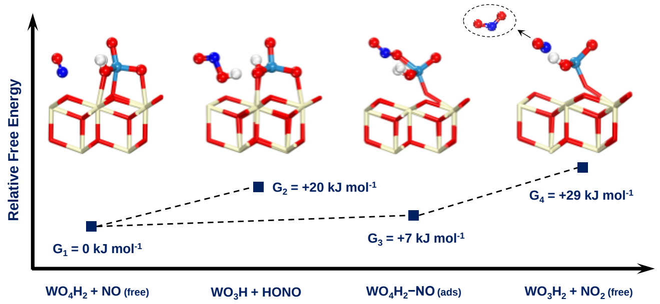

Fig.6. PBE+*U*+D optimized $WO_4H_2/CeO_2$ (111) with a free NO close to $WO_4H_2$, HONO formation, NO adsorption and $NO_2$ release (from left to right). Gibbs free energies at 473 K and standard pressure (0.1 MPa) are also reported. $Ce^{4+}$: ivory, W: dodger blue, H: white, N: blue, O: red, respectively.

## CONCLUSION

In this work, we use $WO_3$-promoted $CeO_2$, i.e., $WO_3/CeO_2$, known as preeminent in LT-SCR reactions, as a model $CeO_2$-based SCR catalyst, and combine kinetic, characteristic and in situ spectroscopic measurements with theoretical treatments to reveal the mechanistic connections between NO oxidative activation and LT-SCR turnovers. The present results demonstrate that NO oxidation to $NO_2$ is both kinetically (reaction rates: 8~40-fold lower than LT-SCR at 423~523 K) and thermodynamically (reaction free energy at 473 K: ~20 kJ mol$^{-1}$ higher than NO to nitrites) less favorable than NO activation to nitrite-species, thus suggesting a relevance of the latter route, rather than NO oxidation to $NO_2$ and subsequent occurrence of fast SCR, to $WO_3/CeO_2$-catalyzed LT-SCR reaction cascade. These mechanistic discussions progress the understanding of the inextricable connections between the superior redox property of ceria-based SCR catalysts and their promoted LT-SCR activities.

## ACKNOWLEDGEMENT

The authors acknowledge the financial support from National Natural Science Foundation of China (Grant: 51836006, 52006192).

## REFERENCE

[1] Jaegers NR, Lai JK, He Y, Walter E, Dixon DA, Vasiliu M, et al. Mechanism by which Tungsten Oxide Promotes the Activity of Supported V2 O5 /TiO2 Catalysts for NOX Abatement: Structural Effects Revealed by (51) V MAS NMR Spectroscopy. Angewandte Chemie. 2019;58:12609-16.

[2] Tronconi E, Nova I, Ciardelli C, Chatterjee D, Weibel M. Redox features in the catalytic mechanism of the "standard" and "fast" NH3-SCR of NOx over a V-based catalyst investigated by dynamic methods. J Catal. 2007;245:1-10.

[3] Paolucci C, Khurana I, Parekh AA, Li S, Shih AJ, Li H, et al. Dynamic multinuclear sites formed by mobilized copper ions in NO x selective catalytic reduction. Science. 2017;357:898-903.

[4] Hu WS, Gao X, Deng YW, Qu RY, Zheng CH, Zhu XB, et al. Deactivation mechanism of arsenic and resistance effect of SO42- on commercial catalysts for selective catalytic reduction of NOx with NH3. Chemical Engineering Journal. 2016;293:118-28.

[5] Marberger A, Ferri D, Elsener M, Krocher O. The Significance of Lewis Acid Sites for the Selective Catalytic Reduction of Nitric Oxide on Vanadium-Based Catalysts. Angewandte Chemie. 2016;55:11989-94.

[6] Wang X, Shi Y, Li S, Li W. Promotional synergistic effect of Cu and Nb doping on a novel Cu/Ti-Nb ternary oxide catalyst for the selective catalytic reduction of NO x with NH 3. Applied Catalysis B: Environmental. 2018;220:234-50.

[7] Hu W, Zhang Y, Liu S, Zheng C, Gao X, Nova I, et al. Improvement in activity and alkali resistance of a novel V-Ce(SO4)2/Ti catalyst for selective catalytic reduction of NO with NH3. Appl Catal B. 2017;206:449-60.

[8] Vuong TH, Radnik J, Rabeah J, Bentrup U, Schneider M, Atia H, et al. Efficient VOx/Ce1-xTixO2 Catalysts for Low-Temperature NH3-SCR: Reaction Mechanism and Active Sites Assessed by in Situ/Operando Spectroscopy. Acs Catalysis. 2017;7:1693-705.

[9] Peng Y, Wang CZ, Li JH. Structure-activity relationship of VOx/CeO2 nanorod for NO removal with ammonia. Appl Catal B-Environ. 2014;144:538-46.

[10] Shan W, Liu F, He H, Shi X, Zhang C. Novel cerium-tungsten mixed oxide catalyst for the selective catalytic reduction of NO(x) with NH3. Chem Commun (Camb). 2011;47:8046-8.

[11] Qu RY, Gao X, Cen KF, Li JH. Relationship between structure and performance of a novel cerium-niobium binary oxide catalyst for selective catalytic reduction of NO with NH3. Appl Catal B-Environ. 2013;142:290-7.

[12] Peng Y, Li K, Li J. Identification of the active sites on CeO2–WO3 catalysts for SCR of NOx with NH3: An in situ IR and Raman spectroscopy study. Appl Catal B. 2013;140-141:483-92.

[13] Hu W, Zou R, Dong Y, Zhang S, Song H, Liu S, et al. Synergy of vanadia and ceria in the reaction mechanism of low-temperature selective catalytic reduction of NOx by NH3. J Catal. 2020;391:145-54.

[14] Wang X, Ma H, Li B, Wang Y, Zhang S, Li W, et al. A superior cerium-tungsten bimetal oxide catalyst with flower-like structure for selective catalytic reduction of NO by NH3. Chemical Engineering Journal. 2022;435.

[15] Liu ZM, Zhang SX, Li JH, Zhu JZ, Ma LL. Novel V2O5-CeO2/TiO2 catalyst with low vanadium loading for the selective catalytic reduction of NOx by NH3. Appl Catal B-Environ. 2014;158:11-9.

[16] Qu RY, Peng Y, Sun XX, Li JH, Gao X, Cen KF. Identification of the reaction pathway and reactive species for the selective catalytic reduction of NO with NH3 over cerium-niobium oxide catalysts. Catal Sci Technol. 2016;6:2136-42.

[17] Chang HZ, Li JH, Su WK, Shao YK, Hao JM. A novel mechanism for poisoning of metal oxide SCR catalysts: base-acid explanation correlated with redox properties. Chem Commun. 2014;50:10031-4.

[18] Shan WP, Liu FD, He H, Shi XY, Zhang CB. A superior Ce-W-Ti mixed oxide catalyst for the selective catalytic reduction of NOx with NH3. Appl Catal B-Environ. 2012;115:100-6.

[19] Chen L, Li JH, Ge MF, Ma L, Chang HZ. Mechanism of Selective Catalytic Reduction of NOx with NH3 over CeO2-WO3 Catalysts. Chinese J Catal. 2011;32:836-41.

[20] Kresse G, Furthmuller J. Efficient iterative schemes for ab initio total-energy calculations using a plane-wave basis set. Phys Rev B. 1996;54:11169-86.

[21] Perdew JP, Burke K, Ernzerhof M. Generalized gradient approximation made simple. Phys Rev Lett. 1996;77:3865-8.

[22] Dudarev SL, Botton GA, Savrasov SY, Humphreys CJ, Sutton AP. Electron-energy-loss spectra and the structural stability of nickel oxide: An LSDA+U study. Phys Rev B. 1998;57:1505-9.

[23] Grimme S, Antony J, Ehrlich S, Krieg H. A consistent and accurate ab initio parametrization of density functional dispersion correction (DFT-D) for the 94 elements H-Pu. J Chem Phys. 2010;132:154104.

[24] Grimme S, Ehrlich S, Goerigk L. Effect of the damping function in dispersion corrected density functional theory. J Comput Chem. 2011;32:1456-65.

[25] Iwaszuk A, Nolan M. Electronic Structure and Reactivity of Ce- and Zr-Doped TiO2: Assessing the Reliability of Density Functional Theory Approaches. The Journal of Physical Chemistry C. 2011;115:12995-3007.

[26] Nolan M. Molecular Adsorption on the Doped (110) Ceria Surface. J Phys Chem C. 2009;113:2425-32.

[27] Kropp T, Paier J, Sauer J. Support effect in oxide catalysis: methanol oxidation on vanadia/ceria. Journal of the American Chemical Society. 2014;136:14616-25.

[28] Hu W, Iacobone U, Gramigni F, Zhang Y, Wang X, Liu S, et al. Unraveling the Hydrolysis of Z2Cu2+ to ZCu2+(OH)− and Its Consequences for the Low-Temperature Selective Catalytic Reduction of NO on Cu-CHA Catalysts. ACS Catalysis. 2021;11:11616-25.

[29] Hu W, Selleri T, Gramigni F, Fenes E, Rout KR, Liu S, et al. On the Redox Mechanism of Low-Temperature NH3 -SCR over Cu-CHA: A Combined Experimental and Theoretical Study of the Reduction Half Cycle. Angewandte Chemie. 2021;60:7197-204.

[30] Ruggeri MP, Selleri T, Colombo M, Nova I, Tronconi E. Identification of nitrites/HONO as primary products of NO oxidation over Fe-ZSM-5 and their role in the Standard SCR mechanism: A chemical trapping study. J Catal. 2014;311:266-70.

[31] Ruggeri MP, Selleri T, Colombo M, Nova I, Tronconi E. Investigation of NO2 and NO interaction with an Fe-ZSM-5 catalyst by transient response methods and chemical trapping techniques. J Catal. 2015;328:258-69.

[32] Busca G, Lietti L, Ramis G, Berti F. Chemical and mechanistic aspects of the selective catalytic reduction of NOx by ammonia over oxide catalysts: A review. Appl Catal B-Environ. 1998;18:1-36.

[33] Michalow-Mauke KA, Lu Y, Kowalski K, Graule T, Nachtegaal M, Krocher O, et al. Flame-Made WO3/CeOx-TiO2 Catalysts for Selective Catalytic Reduction of NOx by NH3. Acs Catalysis. 2015;5:5657-72.

[34] Philipp S, Drochner A, Kunert J, Vogel H, Theis J, Lox ES. Investigation of NO adsorption and NO/O2 co-adsorption on NOx-storage-components by DRIFT-spectroscopy. Top Catal. 2004;30-1:235-8.

[35] Selleri T, Nova I, Tronconi E. The low-temperature interaction of NH3/NO/NO2+O2 with Fe-ZSM-5+BaO/Al2O3 and H-ZSM-5+BaO/Al2O3: Influence of phase separation and relevance for the NH3-SCR chemistry. Appl Catal B-Environ. 2017;206:471-8.